ACS Sustainable Chemistry & Engineering

Research Article

pubs.acs.org/journal/ascecg

Antibacterial Activity of Graphene Oxide/g-C_3N_4 Composite through Photocatalytic Disinfection under Visible Light

Long Sun,[†] Ting Du,[†] Chao Hu, Juanni Chen, Jian Lu, Zhicheng Lu, and Heyou Han*

State Key Laboratory of Agricultural Microbiology, College of Science, College of Food Science and Technology, Huazhong Agricultural University, Wuhan 430070, PR China

Supporting Information

ABSTRACT: Carbon-based nanomaterials have been widely developed into innovative antimicrobial agents due to their advantages of high surface-to-volume ratio, extremely high mechanical strength, and distinct physicochemical properties. Here, the nanocomposite of graphene oxide/graphitic carbon nitride (GO/g-C_3N_4), a free-metal photocatalyst, was fabricated through sonication at room temperature and its antibacterial activity against *Escherichia coli* (*E. coli*) was investigated. The 100 μg/mL GO/g-C_3N_4 composite was found to kill 97.9% of *E. coli* after 120 min visible light irradiation, which was further confirmed by fluorescent-based cell membrane integrity assay. Additionally, the holes produced by photocatalysis were confirmed by electron spin resonance (ESR) spectra and trapping experiments to participate in photocatalytic sterilization as principal active species and were further verified by transmission electron microscopy (TEM) and scanning electron microscope (SEM) to lead to the distortion and rupture of cell membrane and finally cell death. Further photoluminescence (PL) spectra, cyclic voltammetry, photocurrent generation, and impedance spectroscopy (EIS) characterization revealed that the introduction of GO contributed to separate photogenerated electrons and prevents the electron−hole pairs of g-C_3N_4 from recombing to generate more h^+, thus directly improving the bactericidal ability of GO/g-C_3N_4. Reusability assays indicated that the GO/g-C_3N_4 retained more than 90% of activity after four cycles of use. This study facilitates an in-depth understanding of the mechanism of visible light-driven disinfection and provides an ideal candidate sterilizing agent for treating microbial-contaminated water.

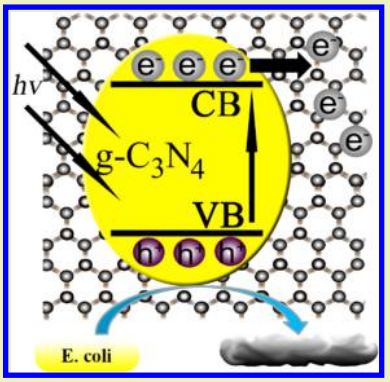

KEYWORDS: *GO/g-C_3N_4, Escherichia coli, Photocatalytic disinfection, Metal-free photocatalyst*

INTRODUCTION

Currently, the number of people lacking access to clean water has reached nearly 900 million in the world, and about 1.5 million children under the age of five lose their lives due to the use of unsafe drinking water every year.[1] The content of *Escherichia coli* (*E. coli*) is an important indicator of clean water. Drinking water containing excessive amounts of *E. coli* can lead to severe inflammation and even death. Commonly used water disinfection methods include chemical and physical ones, such as the use of chlorine, chlorine dioxide, ozone, and UV irradiation. Despite effective elimination of microbial contamination, these methods have several common drawbacks. For instance, chlorination is not environmentally friendly due to its association with carcinogenic byproducts, such as trihalomethanes.[2] UV light disinfection is not sustainable, and when the water leaves the ultraviolet sterilization device, the surviving bacteria will breed rapidly and lead to secondary pollution. Besides, some UV-resistant *E. coli* strains can hardly be killed by UV light. Therefore, it is highly necessary to develop novel antimicrobial agents for effective treatment of microbial-contaminated water.

Nanoscale materials have sprung up as innovative antimicrobial agents because of their unique chemical and physical properties. Up to now, TiO_2,[3] ZnO, MgO, Al_2O_3, AgNPs,[4,5] and carbon-based nanomaterials[6−8] (GO, rGO, SWCNT, C60, MWCNT) have been reported to display antibacterial activity to some extent, and among them, TiO_2 has attracted wide attention in the photocatalysis field. However, pure TiO_2 is not an ideal photocatalyst due to its limitations in the excitation wavelength of ultraviolet band, implying that it can not make full use of solar light.[9] To solve this problem, TiO_2 was modified with noble metal,[10] metal oxide,[11] and semiconductor.[12] It was reported that *E. coli* could be killed when cultured with TiO_2/Pt particles for 60−120 min under metal halide lamp irradiation.[13] Wen et al. also reported that a new nanocomposite prepared from anatase TiO_2, Ag, and graphene showed a notable increase in both visible light absorption and photocatalytic activity.[14] However, the majority of previously reported photocatalysts for bacterial inactivation contain metal nanoparticles and ions, such as Ag^0,[15] Ag^+, and Cu^{2+}, which are unfavorable for "green" water disinfection.[16]

Graphitic carbon nitride (g-C_3N_4) is a metal-free photocatalyst consisting of tri-s-triazine subunits which are linked by planar tertiary amino groups in a layer, and it has attracted

Received: May 7, 2017
Revised: August 6, 2017
Published: August 23, 2017

DOI: 10.1021/acssuschemeng.7b01431
ACS Sustainable Chem. Eng. XXXX, XXX, XXX−XXX

extensive interest among researchers due to its high photochemical stability,[17] plentiful material source, inexpensive synthesis, and nontoxicity.[18] These superior properties demonstrate the potential of metal-free g-C_3N_4 as a "sustainable" advanced photocatalyst, but pure g-C_3N_4 still has some limitations in photocatalytic efficiency because of its low electrical conductivity and rapid recombination frequency of photogenerated carriers.[19] One intriguing method for improving the separation efficiency is to build heterojunction with graphene oxide (GO).[20,21] Go has been served as a separation focus and electron acceptor to enhance the efficiency of light collection and electron-hole separation.[22,23] When combined with g-C_3N_4, GO can rapidly transfer the photogenerated electrons to the surrounding environment, leaving little chance for the photogenerated electrons and holes to recombine.[24,25] Recently, GO/g-C_3N_4 nanocompsites have been widely explored for the application as organic electrocatalysts in oxygen evolution reaction,[20,26] reduction of carbon dioxide to methane,[27,28] photoelectrochemical sensing,[29,30] fuel cell catalysis,[31,32] H_2 production,[33] and pollutant degradation.[34,35] However, to our best knowledge, little literature is available about the function of GO/g-C_3N_4 as an antibacterial agent.

In this present study, we synthesized a nonmetal heterojuntion photocatalyst GO/g-C_3N_4 (containing 1 wt % GO) composite by sonication at room temperature and investigated its antibacterial ability on *E. coli*. Bacterial survival analyses demonstrated that GO/g-C_3N_4 composite could kill 97.9% of *E. coli* after 120 min visible light irradiation at the concentration of 100 μg/mL. The antibacterial activity of GO/g-C_3N_4 composite might be derived from the holes with positive charge (h^+) produced by photocatalysis, which lead to the distortion and rupture of cell membrane (Scheme 1).

EXPERIMENTAL SECTION

Chemicals. In this work, graphite powder, urea, NaCl, yeast extract, tryptone, Cr (VI), and sodium oxalate were of analytical grade and utilized as purchased without further purification. Chemicals were purchased from Aladdin Corporation (Shanghai, China). The *E. coli* strains were maintained by the State Key Laboratory of Agricultural Microbiology of Huazhong Agricultural University.

Scheme 1. Possible Mechanisms of the Antibacterial Activity of GO/g-C_3N_4 Composite

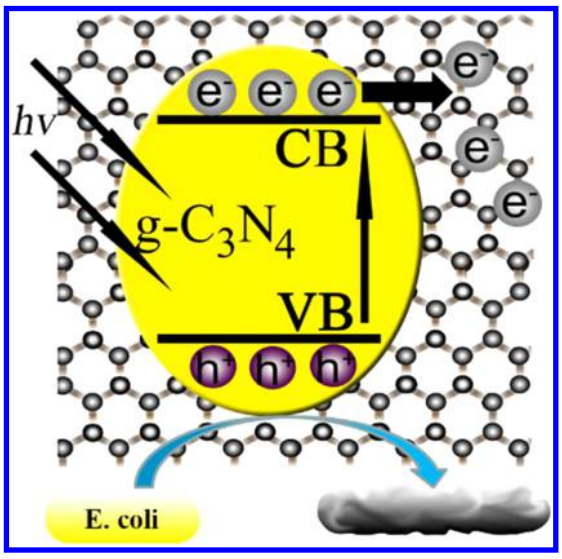

Synthesis of GO. GO was synthesized from natural graphite powders according to the typical Hummers method with minor modification.[36] Briefly, 1.0 g of nature graphite power was mixed with 23 mL sulfuric acid (95%) under ice bath, followed by addition of 3.0 g $KMnO_4$ under vigorous stirring to ensure thorough dissolution. After adequate oxidation, the mixture was ultrasonicated at room temperature for 10 h. Next, the mixture was quickly transferred into 46 mL H_2O and 150 mL H_2O_2 solution (9%). Finally, the solution was filtered, washed with 0.2 M HCl, and freeze-dried for 12 h for further use.

Synthesis of g-C_3N_4. The g-C_3N_4 was prepared by heating urea directly.[37] Three grams of urea powder were heated to 600 °C at a rate of 5 °C per minute. After 4 h of heating, the urea sample was cooled down to room temperature and then ground to powder.

Fabrication of GO/g-C_3N_4 Composite. The GO/g-C_3N_4 composite photocatalyst was prepared by a straightforward sonochemical method. First, 100 mg g-C_3N_4 was suspended in 80 mL ultrapure water while 1.0 mg GO was mixed with 20 mL ultrapure water. Then, the two solutions were ultrasonicated separately for 1 h. Next, the GO and g-C_3N_4 dispersions were mixed and ultrasonicated for 2 h. After freeze-drying for 24 h, the product was obtained.

Characterization of GO/g-C_3N_4 Composite. The morphology of the as-prepared photocatalysts was characterized via transmission electron microscopy (TEM), with the images obtained through a Hitachi H-7650 EM operated at 300 kV. The crystal structures were measured by X-ray diffractometer (XRD) using Cu−Kα radiation. The surface functional groups of obtained samples were investigated via Fourier transform infrared spectroscopy (FT-IR, Nicolet Avatar-330) using the KBr pellet pressing method. Synergetic effects of GO and g-C_3N_4 on light absorption properties were studied using UV−vis diffuse reflectance spectroscopy (DRS, Cary 5000 UV−vis-NIR) with an integrating sphere using $BaSO_4$ as the blank reference. The photoluminescence (PL, Hitachi F-4600) spectral analysis was performed to probe the effect of the GO modification. Photocurrent, cyclic voltammograms and electrochemical impedance spectral (EIS) tests were performed by a CHI 660D electrochemical workstation (Chenhua Instrument, Shanghai, China), using Pt foil as a counter electrode, Ag/AgCl (saturated KCl) as a reference electrode, and 0.1 M Na_2SO_4 solution as the electrolyte. X-ray photoelectron spectra (XPS) were measured using a Thermo VG Multilb 2000 spectrometer with a homochromous Al−Kα radiation source.

Antibacterial Activity Test. *E. coli* was applied to assess the antibacterial effect of GO/g-C_3N_4 composite. Briefly, 3.0 μL of *E. coli* was added into 3.0 mL LB liquid medium, which was then transferred into a 37 °C incubator with gentle shaking. After 16 h incubation, the cell count approximated 10^9 colony forming units (CFU) per milliliter. Then bacterial cells were collected by centrifugation at 5000 rpm for 10 min, followed by washing three times to remove the supernatant, and then resuspended in PBS buffer (pH = 7.4). The bacterial suspensions were diluted to 10^7 CFU/mL.

Next, 100 μL composite photocatalyst suspensions with different concentrations were added to 3.0 mL of bacterial solutions to ensure that the ultimate concentrations of the GO/g-C_3N_4 composite were 25, 50, and 100 μg/mL. Then the mixture was treated for 2 h under a 300 W xenon lamp mounted with UV filter (λ < 420 nm). Meanwhile, the light intensity was maintained at 300 mW/cm^{-1} throughout the experiments. The antibacterial experiment was conducted at room temperature by constantly stirring the mixture at 500 rpm and collecting 100 μL sample from the mixture per 30 min. After dilution to a suitable concentration with PBS buffer, 100 μL diluted sample was quickly spread on an LB agar culture plate and cultured at 37 °C for 17 h. The survival rate was estimated by the plate count method. The blank control group without any GO/g-C_3N_4 composite and the light control without any irradiation were also prepared. All the experiments were performed in triplicate.

Morphological Analysis of Bacterial Cells. SEM and TEM were often applied to characterize the morphology of *E. coli* untreated and treated with GO/g-C_3N_4 composite under visible light or dark. The

DOI: 10.1021/acssuschemeng.7b01431
ACS Sustainable Chem. Eng. XXXX, XXX, XXX−XXX

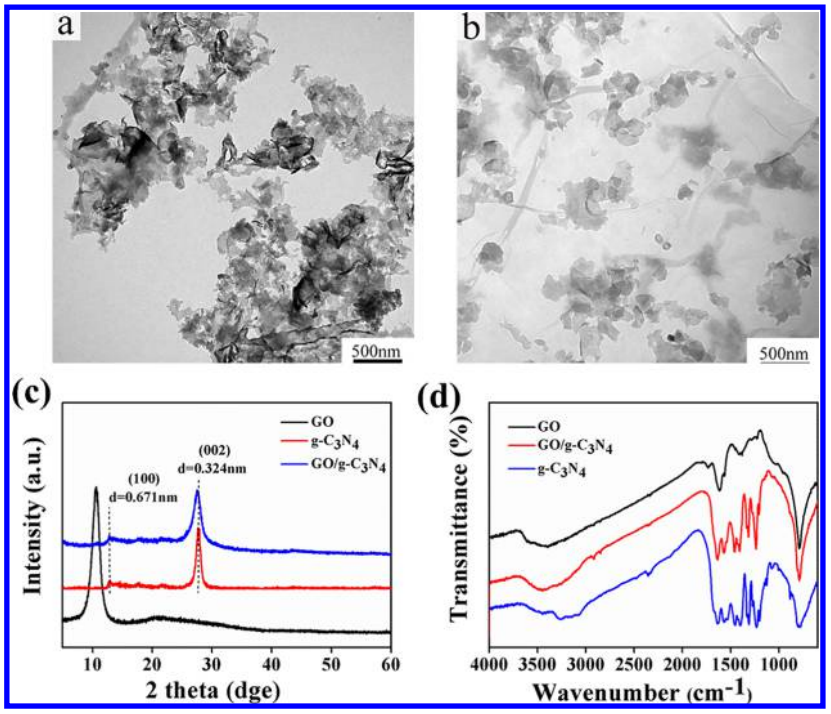

Figure 1. TEM pictures of (a) g-C_3N_4, (b) GO/g-C_3N_4. (c) XRD and (d) FT-IR spectra of GO, g-C_3N_4, and GO/g-C_3N_4.

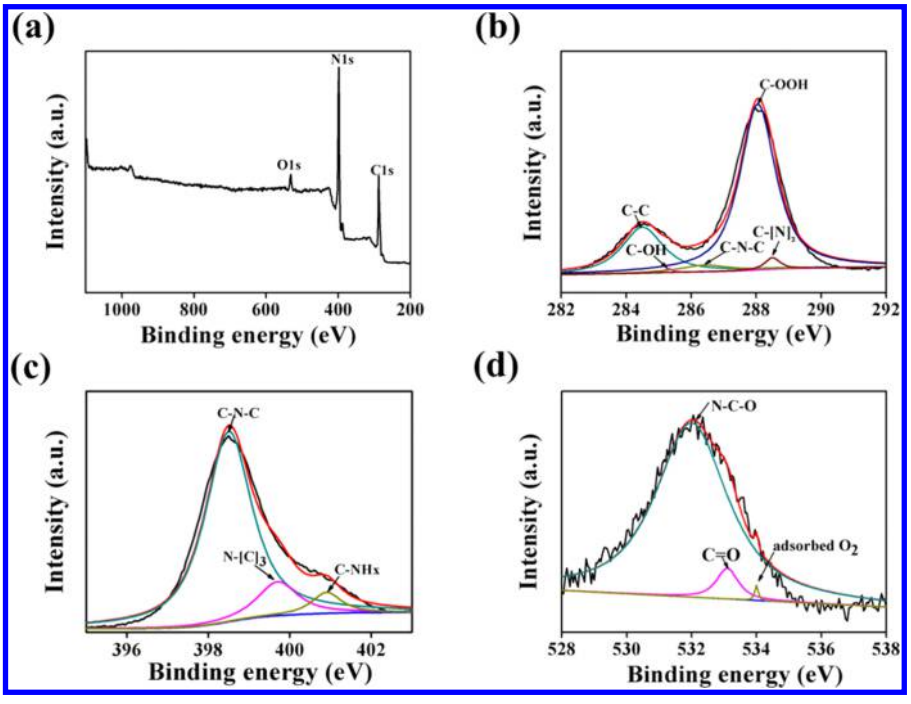

Figure 2. XPS spectra of GO/g-C_3N_4: (a) survey spectrum, (b) C 1s spectrum, (c) N 1s spectrum, and (d) O 1s spectrum.

bacterial suspensions were exposed to GO/g-C_3N_4 under irradiation for 2 h, then centrifugated at 8000 rpm for 5 min. Next, the condensed cells were fixed with cold 2.5% glutaraldehyde for 1 h, washed twice with PBS buffer, dehydrated successively with 30, 50, 70, 90, and 100% ethanol for 15 min and then freeze-dried. Finally, the obtained samples were observed separately under a SEM (JEOL JSM-6700F) and TEM (HITACHI H-7650).

Fluorescent-Based Cell Membrane Integrity Analysis. *E. coli* cells in logarithmic phase were cultured in LB medium, followed by mock-treatment or treatment with 100 μg/mL GO/g-C_3N_4 composite under visible light for 2 h. The cells were collected by centrifugating, followed by staining with propidium iodide (PI, 10 μg/mL) and 4′-6-diamidino-2-phenylindole (DAPI, 5 μg/mL) for 15 and 5 min, respectively. After washing twice to discard the excess dye, the bacterial cells were observed with a confocal microscope (OLYMPUS FV1000).

Cytotoxicity Test. Five $\times 10^3$ cells/well Hela cells in 96-well plates were cultured until 80−90% confluence, followed by supplementation of different concentrations (5, 10, 20, 50, 100, and 200 μg/mL) of GO/g-C_3N_4. After 24 h incubation, each well was supplemented with 20 μL MTT reagent (3-(4,5-dimethyl-2-thiazolyl)-2,5-diphenyl-2-*H*-tetrazolium bromide) and cultured for another 4 h. Then the supernatant was discarded, and the formazan was dissolved in 150 μL dimethyl sulfoxide (DMSO). Finally, absorbance at 490 nm was

DOI: 10.1021/acssuschemeng.7b01431
ACS Sustainable Chem. Eng. XXXX, XXX, XXX−XXX

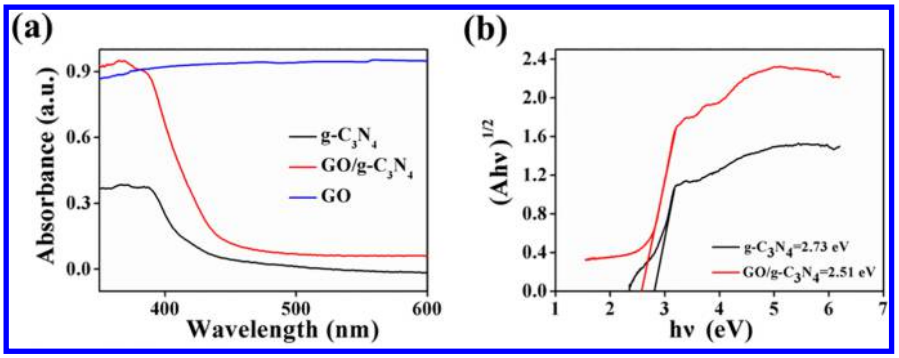

Figure 3. (a) UV−vis diffuse reflectance images of pure g-C_3N_4, GO, and GO/g-C_3N_4 nanocomposites. (b) Plots of converted Kubelka−Munk functions versus light energy.

determined by an enzyme linked immunosorbent assay (ELISA) microplate reader.[38]

RESULTS AND DISCUSSION

Characterization of GO/g-C_3N_4. Figure 1 shows the morphology and microstructure of the GO/g-C_3N_4 (containing 1 wt % GO) composite characterized by TEM, XRD, and FT-IR. As displayed in Figure 1a and b, g-C_3N_4 was well spread and attached to GO, and its size was in the range of tens to hundreds of nanometers. In the XRD of GO, g-C_3N_4 and GO/g-C_3N_4 (Figure 1c), the peak at 10.30° of GO was attributed to the interlayer spacing (001) diffraction peak, with an interlayer spacing distance of 0.86 nm.[39,40] The g-C_3N_4 had two intensive peaks at 13.12° and 27.50°. The former represented the (100) diffraction peak of in-plane structural packing motif of tris-triazine units, and the packing distance was 0.671 nm, while the latter represented an interlayer stacking (002) diffraction peak of aromatic segments, and the stacking distance was 0.324 nm.[41] There was no obvious difference between g-C_3N_4 and GO/g-C_3N_4 in scanning spectra, suggesting no effect of the modification with 1% GO on the g-C_3N_4 lattice structure.[42]

The surface functional groups of GO, g-C_3N_4, and GO/g-C_3N_4 were measured by the Fourier transform infrared (FTIR) spectroscopy. In Figure 1d, the wider band at 3250−3750 cm^{-1} of GO was attributed to the stretching vibrations of −OH and the physically absorbed H_2O; the high-intensity peaks around 1735 and 1612 cm^{-1} to the C═O stretching vibration and distortion vibration of intercalated water; the bands at 1414, 1224, and 1046 cm^{-1} to the C−O, C−OH, and C−O−C bonds, respectively; the peak around 789 cm^{-1} to the absorption of epoxide group;[43] the peaks at 1637, 1571, 1404, 1318, and 1238 cm^{-1} of pure g-C_3N_4 to the characteristic stretching vibrations of C−N heterocycles; and the peak at 814 cm^{-1} to the typical stretching vibration of triazine units.[44] For the GO/g-C_3N_4 composite, due to the low GO content in the composite, the representative peaks of CN heterocycles could be only observed in the spectrum of g-C_3N_4.

The chemical structure of of GO/g-C_3N_4 was examined by X-ray photoelectron spectroscopy (XPS). In Figure 2b, the notably unsymmetrical and obvious C 1s peaks showed the coexistence of diacritical matrix, and the C 1s peaks at 284.7, 285.2, 286.4, 288.1, and 288.5 eV could represent sp^2-hybridized carbons (C−C), C−OH, C−N−C, C═O−OH, and C−$(N)_3$ bonds, respectively, through signal deconvolution via Gaussian curve fitting.[45−47] The N 1s peak at 398.5 eV was assigned to the sp^2 N contained in triazine rings, and the peaks at 399.8 and 401 eV were attributed to the N−$(C)_3$ and −NH_2 or ═NH groups (Figure 2c).[48] The O 1s peaks at 532 and 533 eV were associated with O−C−N and O═C bonds, while the peak at 540 eV was due to the adsorbed O_2 (Figure 2d).[49]

Optical Property. Optical properties and band positions of samples were investigated using UV−vis diffuse reflectance spectroscopy and Mott−Schottky plots. In Figure 3a, the band gap absorption edge of both g-C_3N_4 and GO/g-C_3N_4 was around 460 nm, suggesting carbon was not contained in the g-C_3N_4 lattice and that the GO sheet was only used as a matrix to fix g-C_3N_4 nanosheets.[22] In addition, GO/g-C_3N_4 showed strong absorption over the whole range of the investigated wavelengths, which resulted from the strong absorption of GO in visible light region.[24] Besides, the band gap energies were estimated to be 2.73 and 2.51 eV for g-C_3N_4 and GO/g-C_3N_4 (Figure 3b). The narrowing band gap and enhanced visible light utilization of the nanocomposites can be ascribed to graphene hybridization, which could result in the electronic transition between g-C_3N_4 and graphene. rGO modification in g-C_3N_4 has been reported to improve light utilization and thus photocatalytic efficiency.[50] Ong et al. also showed that the exceptional enhancement of light absorption and the extension of absorption edge might result from the effect of graphene on the hybrid nanostructures.[27] Our results were similar to the previous reports,[27,50] suggesting that GO enhances the light aggregating efficiency of the GO/g-C_3N_4 composite.

Antibacterial Activity of GO/g-C_3N_4 Composite. *E. coli* was used as a model microorganism to estimate the photocatalytic disinfection ability of GO/g-C_3N_4. As shown in Figure 4, in blank control (under light irradiation without catalysts), there were no bacteria inactivated, suggesting that bright light had no effect on the bacteria. Meanwhile, in the dark treatment (catalysts without light irradiation), no bacterial disinfection was detected, demonstrating the nontoxicity of the

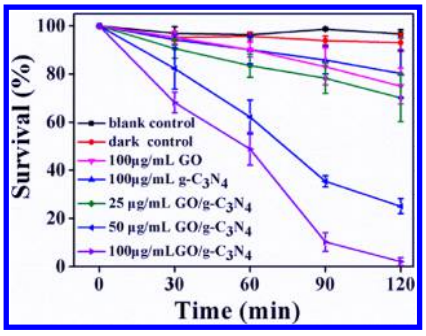

Figure 4. Photocatalytic disinfection ability of GO, g-C_3N_4, and GO/g-C_3N_4. Results were reported as the mean ± SD from three independent experiments.

DOI: 10.1021/acssuschemeng.7b01431
ACS Sustainable Chem. Eng. XXXX, XXX, XXX−XXX

photocatalyst to *E. coli*. In Figure 4, it can also be seen that 100 μg/mL GO had weak disinfection ability, which was consistent with the results of previous literature.[51] At the same concentration, GO/g-C_3N_4 composite showed significantly higher disinfection efficiency than the GO and g-C_3N_4 in killing *E. coli*. After 120 min treatment with GO/g-C_3N_4 composite, the survival rate of *E. coli* was only 2.1%, and the antibacterial ability of GO/g-C_3N_4 against *E. coli* was also dose-dependent.

The reliability of the CFU method in the above test was verified by a fluorescent-based cell live/dead test using the confocal laser scanning fluorescence microscopy imaging system. Bacterial suspension was stained by DAPI and PI fluorescence dye reagent. DAPI can quickly pass through the unbroken membrane of live cells and combine with DNA in nucleus, while PI can only pass through the broken membrane and combine with double strand DNA. In Figure 5a, few dead

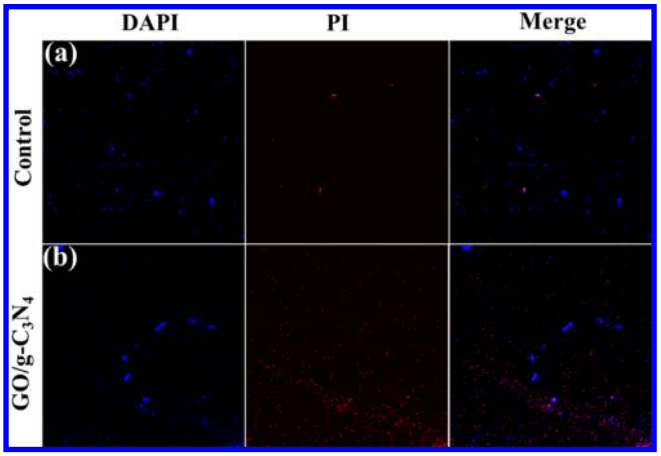

Figure 5. Confocal fluorescent assays of live and dead *E. coli* cells in the absence (a and b) presence of 100 μg/mL GO/g-C_3N_4 under irradiation for 2 h.

cells could be observed in the untreated groups, while in Figure 5b, almost all the *E. coli* cells treated with 100 μg/mL GO/g-C_3N_4 under irradiation for 2 h were stained by PI, suggesting that most *E. coli* cells died due to the rupture of cell membrane.

***E. coli* Structure Observation by SEM and TEM after Treatment with GO/g-C_3N_4 Nanocomposite.** Direct interactions between biological cells and nanomaterials are usually evaluated using scanning electron microscopy (SEM) and transmission electron microscopy (TEM).[40] To observe the changes in the structure of the treated *E. coli*, SEM imaging was performed. In Figure 6a, the control *E. coli* cells were representatively rod-shaped with smooth and intact cell membrane. There were also no obvious changes detected in the morphology of *E. coli* treated with visible light but without GO/g-C_3N_4 composite or treated with GO/g-C_3N_4 in the dark (Figure 6b and c). However, after treatment with GO/g-C_3N_4 under visible light for 120 min, the cell wall became wrinkled, the shape of the cell was completely deformed, and the cell membrane was obviously damaged. In addition, the size of the cells was very uneven, with some cells almost twice longer than others (Figure 6d), and cell elongation is a classical bacterial response to stresses including exposure to biocides. These observations indicated that the visible light (without GO/g-C_3N_4 composite) or GO/g-C_3N_4 composite (in the dark condition) has no effect on *E. coli* cells, but some active species

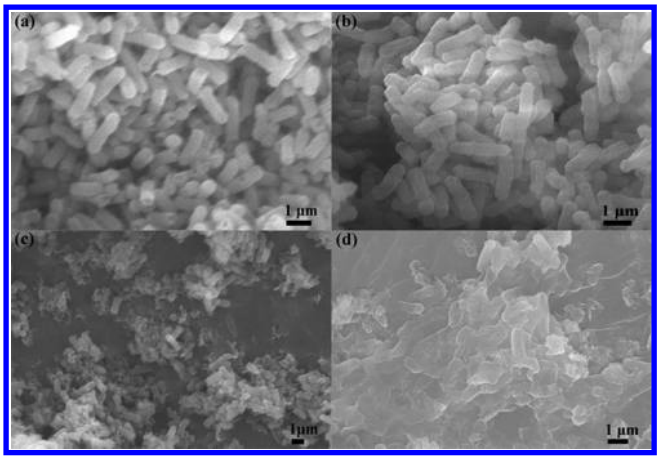

Figure 6. SEM pictures of *E. coli* (a) untreated or treated with (b) visible light but without GO/g-C_3N_4 composite, (c) 100 μg/mL GO/g-C_3N_4 composite in the dark, and (d) 100 μg/mL GO/g-C_3N_4 composite under light irradiation for 2 h. Scare bars: 1 μm.

are generated by GO/g-C_3N_4 composite under light irradiation, such as h^+, $\bullet O_2^-$, and H_2O_2, which interact with the cell membrane and eventually lead to cell death.

The interactions between the *E. coli* and GO/g-C_3N_4 were further confirmed by TEM imaging. In Figure 7a–c, the *E. coli*

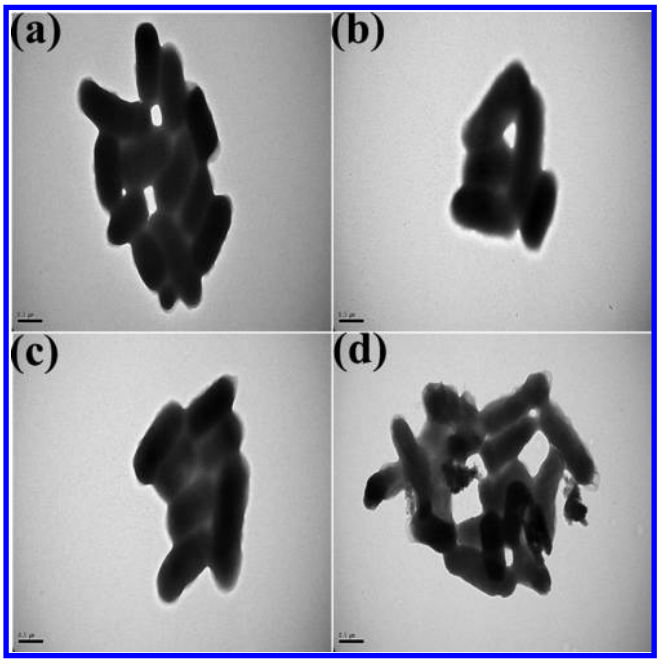

Figure 7. TEM pictures of *E. coli* (a) untreated or treated with (b) visible light but without GO/g-C_3N_4 composite, (c) 100 μg/mL GO/g-C_3N_4 composite in the dark, and (d) 100 μg/mL GO/g-C_3N_4 composite under light irradiation for 2 h. Scale bars: 0.5 μm.

cells untreated, treated with visible light but without GO/g-C_3N_4 composite, or treated with 100 μg/mL GO/g-C_3N_4 in the dark showed the typical rod-shape morphology with an intact structure. However, after 2 h of treatment with 100 μg/mL GO/g-C_3N_4 under irradiation, the bacterial cells were deformed and collapsed and the regular cell structure was destroyed (Figure 7d). These observations were consistent with those of SEM imaging.

DOI: 10.1021/acssuschemeng.7b01431
ACS Sustainable Chem. Eng. XXXX, XXX, XXX−XXX

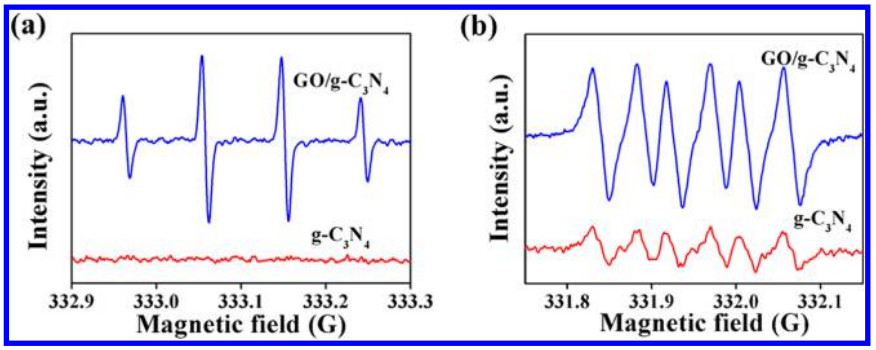

Figure 8. ESR images of (a) DMPO−•OH and (b) DMPO−$•O_2^-$ for g-C_3N_4 and GO/g-C_3N_4 under visible light irradiation.

Cytotoxicity. A good cell compatibility is essential for the use of a composite material as a water disinfectant. The effect of GO/g-C_3N_4 on the viability of Hela cell was evaluated using an MTT cytotoxicity assay. When compared with the control, GO/g-C_3N_4 showed no obvious influence on the proliferation of Hela cell in the 5−100 μg/mL concentration range (Figure S1). Even at the high concentration of 100 μg/mL, the GO/g-C_3N_4 showed little toxicity to cells and the cell viability was still 88%. At 200 μg/mL GO/g-C_3N_4, the cell viability was close to 80%, which was similar to the result of a previous study.[52] In addition, GO/g-C_3N_4 was insoluble in water, it would quickly precipitate at the end of the sterilization experiment, with the residual GO/g-C_3N_4 concentration in the supernatant much lower than the initial GO/g-C_3N_4 concentration. The effect of residual GO/g-C_3N_4 on cell viability was evaluated by centrifuging the supernatant at 10 000 rpm for 15 min, then dissolving the precipitation in cell culture media and using the mixture for cytotoxicity test. As shown in Figure S1, the residual GO/g-C_3N_4 in the supernatant had little effect on cell viability (97%).

Mechanism of Photocatalytic Disinfection. The h^+, $•O_2^-$, •OH, and H_2O_2 produced in the photocatalytic process are generally considered to be the active species for disinfection. Thus, the hydroxyl radical (•OH) and superoxide radical anion ($•O_2^-$) generated by g-C_3N_4 and GO/g-C_3N_4 under visible light irradiation were detected using ESR spin-trap (DMPO) method (Figure 8). As expected, GO/g-C_3N_4 photogenerated more intense typical DMPO−$•O_2^-$ and DMPO−•OH signals than g-C_3N_4, indicating potential participation of $•O_2^-$ and •OH in photocatalytic disinfection. Since the valence band potential of g-C_3N_4 (1.57 V vs NHE) was deficient for oxidation of water or surface hydroxyl group (2.38 V vs NHE) to generate •OH, the strong DMPO−•OH signals implied the further conversion of $•O_2^-$ (Figure 8b).[53]

The dominance of active species during photocatalytic disinfection was examined by employing isopropanol, $K_2Cr_2O_7$, superoxide dismutase (SOD) and soduim oxalate to scavenge hydroxyl radicals (•OH), electron (e^-), superoxide radical anions ($•O_2^-$), and hole (h^+), respectively (Figure 9).[54] With the addition of isopropanol, $K_2Cr_2O_7$ and SOD, only slight changes were detected in the antibacterial ability, suggesting that •OH, e^-, and $•O_2^-$ had no effect on the antibacterial process. However, when sodium oxalate was added, the antibacterial ability was decreased obviously, with a bacterial survival rate of ~60% after 120 min irradiation, indicating that h^+ served as the main active species for photocatalytic sterilization.

Mechanism of Enhanced Photocatalytic Antibacterial Activity. To explore the photocatalytic antibacterial mechanism of g-C_3N_4 and GO/g-C_3N_4, the separation efficiency was studied by photoluminescence (PL) spectroscopy. In Figure 10a, the emission peaks of pure g-C_3N_4 and GO/g-C_3N_4 were around 450 nm, corresponding to the band gap of g-C_3N_4 (2.7 eV).[55] The peak of pure g-C_3N_4 was obviously higher than that of GO/g-C_3N_4, indicating that addition of GO effectively prevented the photogenerated electron−hole pairs from recombination.[24,50] Meanwhile, the CB minimum of g-C_3N_4 was −1.73 eV vs NHE as measured by the cyclic voltammetry method (Figure 10b). These results suggest that the successful electron transfer was due to the reason that Fermi level of GO (−0.08 eV vs NHE) was lower than the CB of g-C_3N_4 resulting from heterojunction formation between g-C_3N_4 and GO, which prevents direct recombination of electrons and holes.[28]

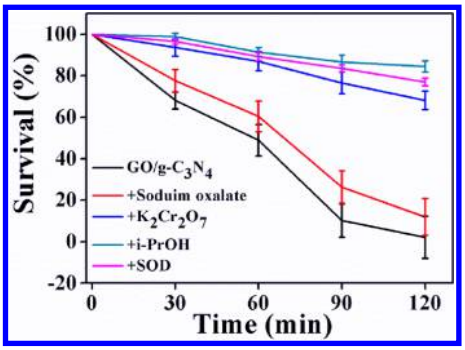

Figure 9. Photocatalytic disinfection ability of GO/g-C_3N_4 with different scavengers (*i*-PrOH → •OH, $K_2Cr_2O_7$ → e^-, SOD → $•O_2^-$, soduim oxalate → h^+). Results were reported as the mean ± SD from three independent experiments.

Photocurrent generation and electrochemical impedance spectroscopy were used to examine the electron generation and charge transfer characteristics of g-C_3N_4, GO and GO/g-C_3N_4. Under visible light (Figure 10c), the photocurrent response of pure g-C_3N_4 was notably lower than that of GO/g-C_3N_4, which was concordant with the result of PL. In Figure 10d, the arc radius on the EIS Nyquist diagram of GO/g-C_3N_4 composites was less than that of pure g-C_3N_4. These results suggested that, under visible light irradiation, GO/g-C_3N_4 showed better charge transport characteristics than g-C_3N_4, which may facilitate charge transfer.

Stability of GO/g-C_3N_4 Photocatalyst. A vital indicator for the practical application of a photocatalyst is stability. In this study, the stability of GO/g-C_3N_4 for the photocatalytic disinfection of *E. coli* under visible light was tested by four cycles of use of the photocatalyst under the same condition. Specifically, the photocatalyst was recollected by centrifuging and the new bacterial suspension was used in each cycle. As

DOI: 10.1021/acssuschemeng.7b01431
ACS Sustainable Chem. Eng. XXXX, XXX, XXX−XXX

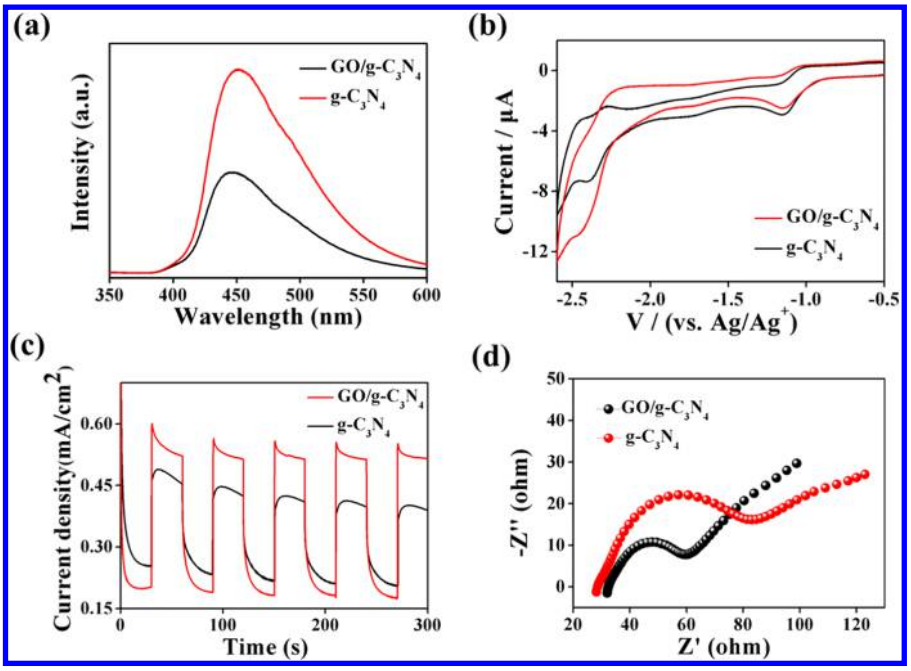

Figure 10. Photoluminescence spectra (a), cyclic voltammograms (b), photocurrent responses (c), and electrochemical impedance spectra (d) of g-C_3N_4, GO and GO/g-C_3N_4 in 0.1 M Na_2SO_4 aqueous solution under visible light irradiation.

shown in Figure 11, the photocatalyst exhibited stable and high photocatalytic disinfection performance in the four cycles.

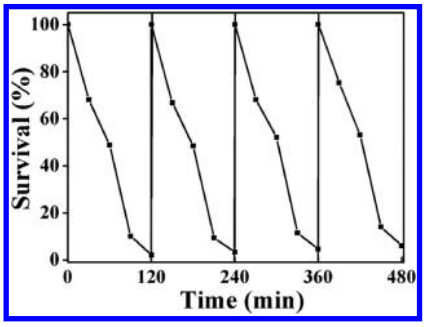

Figure 11. Repeated experiments of photocatalytic disinfection of 100 μg/mL GO/g-C_3N_4 under visible light.

CONCLUSIONS

In this study, GO/g-C_3N_4 composite (containing 1 wt % GO) was successfully synthesized by a facile sonochemical method, and analyzed by standard spectroscopic techniques (UV−vis diffuse reflectance, photoluminescence, XRD, and FTIR spectrosopy) as well as XPS and TEM. The uniform distribution of GO sheets in the layered g-C_3N_4 structure suggest a negligible influence of GO modification on the g-C_3N_4 lattice structure. This is probably the first report to demonstrate that GO/g-C_3N_4 has superior antibacterial activity against *E.coli*. At 100 μg/mL, the GO/g-C_3N_4 composite could kill 97.9% of *E. coli* after 120 min visible light irradiation. The holes (h^+) produced by photocatalysis were confirmed to be the major active species for photocatalytic sterilization and might cause the distortion and rupture of cell membrane. Further analyses revealed that the introduction of GO not only reinforced light absorption and photocurrent but also largely improved the photogenerated electron−hole separation, leading to an increase of the number of holes. Furthermore, GO/g-C_3N_4 exhibited stable and high photocatalytic disinfection efficiency even after four cycles of use. These encouraging results provide experimental basis for further development of GO/g-C_3N_4 composite as an ideal photocatalyst for water sterilization.

ASSOCIATED CONTENT

Supporting Information

The Supporting Information is available free of charge on the ACS Publications website at DOI: 10.1021/acssuschemeng.7b01431.

MTT results for Hela cells exposed to various concentrations of GO/g-C_3N_4 (PDF)

AUTHOR INFORMATION

Corresponding Author

*E-mail: hyhan@mail.hzau.edu.cn (H.H.).

ORCID

Heyou Han: 0000-0001-9406-0722

Author Contributions

†These authors contributed equally.

Notes

The authors declare no competing financial interest.

ACKNOWLEDGMENTS

This work financially supported by the National Natural Science Foundation of China (21375043, 21778020), National Key R & D Program (2016YFD0500700), and Sci-tech Innovation Foundation of Huazhong Agriculture University (2662017PY042). We are also thankful to Prof. Hanchang Zhu for editing of the language.

REFERENCES

(1) Richardson, S. D.; Plewa, M. J.; Wagner, E. D.; Schoeny, R.; DeMarini, D. M. Occurrence, Genotoxicity, and Carcinogenicity of Regulated and Emerging Disinfection By-Products in Drinking Water:

DOI: 10.1021/acssuschemeng.7b01431
ACS Sustainable Chem. Eng. XXXX, XXX, XXX−XXX

A Review and Roadmap for Research. *Mutat. Res., Rev. Mutat. Res.* **2007**, *636*, 178−242.
(2) Hrudey, S. E. Chlorination Disinfection By-Products, Public Health Risk Tradeoffs and Me. *Water Res.* **2009**, *43*, 2057−2092.
(3) Zhang, P.; Cui, H.; Zhong, X.; Li, L. Effects of Nano-TiO_2 Semiconductor Sol on Prevention from Plant Diseases. *Nanoscience* **2007**, *12*, 1−6.
(4) Jo, Y. K.; Kim, B. H.; Jung, G. Antifungal Activity of Silver Ions and Nanoparticles on Phytopathogenic Fungi. *Plant Dis.* **2009**, *93*, 1037−1043.
(5) Lamsal, K.; Kim, S. W.; Jung, J. H.; Kim, Y. S.; Kim, K. S.; Lee, Y. S. Application of Silver Nanoparticles for the Control of Colletotrichum Species in Vitro and Pepper Anthracnose Disease in Field. *Mycobiology* **2011**, *39*, 194−199.
(6) Qu, F.; Li, T.; Yang, M. Colorimetric Platform for Visual Detection of Cancer Biomarker Based on Intrinsic Peroxidase Activity of Graphene Oxide. *Biosens. Bioelectron.* **2011**, *26*, 3927−3931.
(7) Chen, J.; Wang, X.; Han, H. A New Function of Graphene Oxide Emerges: Inactivating Phytopathogenic Bacterium Xanthomonas Oryzae pv. Oryzae. *J. Nanopart. Res.* **2013**, *15*, 1658.
(8) Chen, J.; Peng, H.; Wang, X.; Shao, F.; Yuan, Z.; Han, H. Graphene Oxide Exhibits Broad-Spectrum Antimicrobial Activity Against Bacterial Phytopathogens and Fungal Conidia by Intertwining and Membrane Perturbation. *Nanoscale* **2014**, *6*, 1879−1889.
(9) Mor, G. K.; Varghese, O. K.; Paulose, M.; Shankar, K.; Grimes, C. A. A Review on Highly Ordered, Vertically Oriented TiO_2 Nanotube Arrays: Fabrication, Material Properties, and Solar Energy Applications. *Sol. Energy Mater. Sol. Cells* **2006**, *90*, 2011−2075.
(10) Yu, J.; Xiong, J.; Cheng, B.; Liu, S. Fabrication and Characterization of Ag-TiO_2 Multiphase Nanocomposite Thin Films with Enhanced Photocatalytic Activity. *Appl. Catal., B* **2005**, *60*, 211−221.
(11) Yu, X.; Liu, S.; Yu, J. Superparamagnetic γ-Fe_2O_3@SiO_2@TiO_2 Composite Microspheres with Superior Photocatalytic Properties. *Appl. Catal., B* **2011**, *104*, 12−20.
(12) Robel, I.; Subramanian, V.; Kuno, M.; Kamat, P. V. Quantum Dot Solar Cells. Harvesting Light Energy with CdSe Nanocrystals Molecularly Linked to Mesoscopic TiO_2 Films. *J. Am. Chem. Soc.* **2006**, *128*, 2385−2393.
(13) Pelaez, M.; Nolan, N. T.; Pillai, S. C.; Seery, M. K.; Falaras, P.; Kontos, A. G.; Dunlop, P. S. M.; Hamilton, J. W. J.; Byrne, J. A.; O'Shea, K.; Entezari, M. H.; Dionysiou, D. D. A Review on the Visible Light Active Titanium Dioxide Photocatalysts for Environmental Applications. *Appl. Catal., B* **2012**, *125*, 331−349.
(14) Wen, Y.; Ding, H.; Shan, Y. Preparation and Visible Light Photocatalytic Activity of Ag/TiO_2/Graphene Nanocomposite. *Nanoscale* **2011**, *3*, 4411−4417.
(15) Wang, Y.; Ding, X.; Chen, Y.; Guo, M.; Zhang, Y.; Guo, X.; Gu, H. Antibiotic-Loaded, Silver Core-Embedded Mesoporous Silica Nanovehicles as a Synergistic Antibacterial Agent for the Treatment of Drug-Resistant Infections. *Biomaterials* **2016**, *101*, 207−216.
(16) Fu, F.; Wang, Q. Removal of Heavy Metal Ions from Wastewaters: A Review. *J. Environ. Manage.* **2011**, *92*, 407−418.
(17) Wang, Z.; Guan, W.; Sun, Y.; Dong, F.; Zhou, Y.; Ho, W. K. Water-Assisted Production of Honeycomb-Like g-C_3N_4 with Ultralong Carrier Lifetime and Outstanding Photocatalytic Activity. *Nanoscale* **2015**, *7*, 2471−2479.
(18) Xu, L.; Huang, W. Q.; Wang, L. L.; Tian, Z. A.; Hu, W.; Ma, Y.; Wang, X.; Pan, A.; Huang, G. F. Insights into Enhanced Visible-Light Photocatalytic Hydrogen Evolution of g-C_3N_4 and Highly Reduced Graphene Oxide Composite: The Role of Oxygen. *Chem. Mater.* **2015**, *27*, 1612−1621.
(19) Aleksandrzak, M.; Kukulka, W.; Mijowska, E. Graphitic Carbon Nitride/Graphene Oxide/Reduced Graphene Oxide Nanocomposites for Photoluminescence and Photocatalysis. *Appl. Surf. Sci.* **2017**, *398*, 56−62.
(20) Tian, J.; Liu, Q.; Asiri, A. M.; Alamry, K. A.; Sun, X. Ultrathin Graphitic C_3N_4 Nanosheets/Graphene Composites: Efficient Organic Electrocatalyst for Oxygen Evolution Reaction. *ChemSusChem* **2014**, *7*, 2125−2130.
(21) Duan, J.; Chen, S.; Jaroniec, M.; Qiao, S. Z. Porous C_3N_4 Nanolayers@N-Graphene Films as Catalyst Electrodes for Highly Efficient Hydrogen Evolution. *ACS Nano* **2015**, *9*, 931−940.
(22) Dai, K.; Lu, L.; Liu, Q.; Zhu, G.; Wei, X.; Bai, J.; Xuan, L.; Wang, H. Sonication Assisted Preparation of Graphene Oxide/graphitic-C_3N_4 Nanosheet Hybrid with Reinforced Photocurrent for Photocatalyst Applications. *Dalton T.* **2014**, *43*, 6295−6299.
(23) Qu, F.; Lu, H.; Yang, M.; Deng, C. Electrochemical Immunosensor Based on Electron Transfer Mediated by Graphene Oxide Initiated Silver Enhancement. *Biosens. Bioelectron.* **2011**, *26*, 4810−4814.
(24) Liao, G.; Chen, S.; Quan, X.; Yu, H.; Zhao, H. Graphene Oxide Modified g-C_3N_4 Hybrid with Enhanced Photocatalytic Capability under Visible Light Rrradiation. *J. Mater. Chem.* **2012**, *22*, 2721−2726.
(25) Kumar, S.; Surendar, T.; Baruah, A.; Shanker, V. Synthesis of a Novel and Stable g-C_3N_4-Ag_3PO_4 Hybrid Nanocomposite Photocatalyst and Study of the Photocatalytic Activity under Visible Light Irradiation. *J. Mater. Chem. A* **2013**, *1*, 5333−5340.
(26) Tian, J.; Ning, R.; Liu, Q.; Asiri, A. M.; Al-Youbi, A. O.; Sun, X. Three-Dimensional Porous Supramolecular Architecture from Ultrathin g-C_3N_4 Nanosheets and Reduced Graphene Oxide: Solution Self-Assembly Construction and Application as a Highly Efficient Metal-Free Electrocatalyst for Oxygen Reduction Reaction. *ACS Appl. Mater. Interfaces* **2014**, *6*, 1011−1017.
(27) Ong, W. J.; Tan, L. L.; Chai, S. P.; Yong, S. T. Graphene Oxide as a Structure-Directing Agent for the Two-Dimensional Interface Engineering of Sandwich-Like Graphene-g-C_3N_4 Hybrid Nanostructures with Enhanced Visible-Light Photoreduction of CO_2 to Methane. *Chem. Commun.* **2015**, *51*, 858−861.
(28) Ong, W. J.; Tan, L. L.; Chai, S. P.; Yong, S. T.; Mohamed, A. R. Surface Charge Modification via Protonation of Graphitic Carbon Nitride (g-C_3N_4) for Electrostatic Self-Assembly Construction of 2D/2D Reduced Graphene Oxide (rGO)/g-C_3N_4 Nanostructures toward Enhanced Photocatalytic Reduction of Carbon Dioxide to Methane. *Nano Energy* **2015**, *13*, 757−770.
(29) Feng, J.; Li, Y.; Li, M.; Li, F.; Han, J.; Dong, Y.; Chen, Z.; Wang, P.; Liu, H.; Wei, Q. A Novel Sandwich-Type Electrochemical Immunosensor for PSA Detection Based on PtCu Bimetallic Hybrid (2D/2D) rGO/g-C_3N_4. *Biosens. Bioelectron.* **2017**, *91*, 441−448.
(30) Li, R.; Liu, Y.; Cheng, L.; Yang, C.; Zhang, J. Photoelectrochemical Aptasensing of Kanamycin Using Visible Light-Activated Carbon Nitride and Graphene Oxide Nanocomposites. *Anal. Chem.* **2014**, *86*, 9372−9375.
(31) Fu, Y.; Zhu, J.; Hu, C.; Wu, X.; Wang, X. Covalently Coupled Hybrid of Graphitic Carbon Nitride with Reduced Graphene Oxide as a Superior Performance Lithium-Ion Battery Anode. *Nanoscale* **2014**, *6*, 12555−12564.
(32) Sher Shah, M. S. A.; Park, A. R.; Rauf, A.; Hong, S. H.; Choi, Y.; Park, J.; Kim, J.; Kim, W. J.; Yoo, P. J. Highly Interdigitated and Porous Architected Ternary Composite of SnS_2, g-C_3N_4, and Reduced Graphene Oxide (rGO) as High Performance Lithium Ion Battery Anodes. *RSC Adv.* **2017**, *7*, 3125−3135.
(33) Xiang, Q.; Yu, J.; Jaroniec, M. Preparation and Enhanced Visible-Light Photocatalytic H_2-Production Activity of Graphene/C_3N_4 Composites. *J. Phys. Chem. C* **2011**, *115*, 7355−7363.
(34) Zhang, H.; Zhao, L.; Geng, F.; Guo, L. H.; Wan, B.; Yang, Y. Carbon Dots Decorated Graphitic Carbon Nitride as an Efficient Metal-Free Photocatalyst for Phenol Degradation. *Appl. Catal., B* **2016**, *180*, 656−662.
(35) Tian, J.; Liu, Q.; Asiri, A. M.; Qusti, A. H.; Al-Youbi, A. O.; Sun, X. Ultrathin Graphitic Carbon Nitride Nanosheets: a Novel Peroxidase Mimetic, Fe Doping-Mediated Catalytic Performance Enhancement and Application to Rapid, Highly Sensitive Optical Detection of Glucose. *Nanoscale* **2013**, *5*, 11604−11609.
(36) Marcano, D. C.; Kosynkin, D. V.; Berlin, J. M.; Sinitskii, A.; Sun, Z.; Slesarev, A.; Alemany, L. B.; Lu, W.; Tour, J. M. Improved Synthesis of Graphene Oxide. *ACS Nano* **2010**, *4*, 4806−4814.

DOI: 10.1021/acssuschemeng.7b01431
ACS Sustainable Chem. Eng. XXXX, XXX, XXX−XXX

(37) Zheng, Y.; Liu, J.; Liang, J.; Jaroniec, M.; Qiao, S. Z. Graphitic Carbon Nitride Materials: Controllable Synthesis and Applications in Fuel Cells and Photocatalysis. *Energy Environ. Sci.* **2012**, *5*, 6717−6731.
(38) Wang, Z.; Dong, K.; Liu, Z.; Zhang, Y.; Chen, Z.; Sun, H.; Ren, J.; Qu, X. Activation of Biologically Relevant Levels of Reactive Oxygen Species by Au/g-C_3N_4 Hybrid Nanozyme for Bacteria Killing and Wound Disinfection. *Biomaterials* **2017**, *113*, 145−157.
(39) Zhang, X. Y.; Li, H. P.; Cui, X. L.; Lin, Y. Graphene/TiO_2 Nanocomposites: Synthesis, Characterization and Application in Hydrogen Evolution from Water Photocatalytic Splitting. *J. Mater. Chem.* **2010**, *20*, 2801−2806.
(40) Chen, J.; Sun, L.; Cheng, Y.; Lu, Z.; Shao, K.; Li, T.; Hu, C.; Han, H. Graphene Oxide-Silver Nanocomposite: Novel Agricultural Antifungal Agent Against Fusarium Graminearum for Crop Disease Prevention. *ACS Appl. Mater. Interfaces* **2016**, *8*, 24057−24070.
(41) Martin, D. J.; Qiu, K.; Shevlin, S. A.; Handoko, A. D.; Chen, X.; Guo, Z.; Tang, J. Highly Efficient Photocatalytic H_2 Evolution from Water Using Visible Light and Structure-Controlled Graphitic Carbon Nitride. *Angew. Chem., Int. Ed.* **2014**, *53*, 9240−9245.
(42) Gu, H.; Zhou, T.; Shi, G. Synthesis of Graphene Supported Graphene-Like C_3N_4 Metal-Free Layered Nanosheets for Enhanced Electrochemical Performance and Their Biosensing for Biomolecules. *Talanta* **2015**, *132*, 871−876.
(43) Ai, B.; Duan, X.; Sun, H.; Qiu, X.; Wang, S. Metal-Free Graphene-Carbon Nitride Hybrids for Photodegradation of Organic Pollutants in Water. *Catal. Today* **2015**, *258*, 668−675.
(44) Yan, S. C.; Li, Z. S.; Zou, Z. G. Photodegradation Performance of g-C_3N_4 Fabricated by Directly Heating Melamine. *Langmuir* **2009**, *25*, 10397−10401.
(45) Xiang, Q.; Yu, J.; Jaroniec, M. Preparation and Enhanced Visible-Light Photocatalytic H_2-Production Activity of Graphene/C_3N_4 Composites. *J. Phys. Chem. C* **2011**, *115*, 7355−7363.
(46) Stankovich, S.; Dikin, D. A.; Piner, R. D.; Kohlhaas, K. A.; Kleinhammes, A.; Jia, Y.; Wu, Y.; Nguyen, S. T.; Ruoff, R. S. Synthesis of Graphene-Based Nanosheets via Chemical Reduction of Exfoliated Graphite Oxide. *Carbon* **2007**, *45*, 1558−1565.
(47) Ge, L.; Han, C. Synthesis of MWNTs/g-C_3N_4 Composite Photocatalysts with Efficient Visible Light Photocatalytic Hydrogen Evolution Activity. *Appl. Catal., B* **2012**, *117*, 268−274.
(48) Ge, L.; Han, C.; Liu, J.; Li, Y. Enhanced Visible Light Photocatalytic Activity of Novel Polymeric g-C_3N_4 Loaded with Ag Nanoparticles. *Appl. Catal., A* **2011**, *409*, 215−222.
(49) Li, J.; Shen, B.; Hong, Z.; Lin, B.; Gao, B.; Chen, Y. A Facile Approach to Synthesize Novel Oxygen-Doped g-C_3N_4 with Superior Visible-Light Photoreactivity. *Chem. Commun.* **2012**, *48*, 12017−12019.
(50) Li, Y.; Zhang, H.; Liu, P.; Wang, D.; Li, Y.; Zhao, H. Cross-Linked g-C_3N_4 /rGO Nanocomposites with Tunable Band Structure and Enhanced Visible Light Photocatalytic Activity. *Small* **2013**, *9*, 3336−3344.
(51) Tang, J.; Chen, Q.; Xu, L.; Zhang, S.; Feng, L.; Cheng, L.; Xu, H.; Liu, Z.; Peng, R. Graphene Oxide-Silver Nanocomposite as a Highly Effective Antibacterial Agent with Species-Specific Mechanisms. *ACS Appl. Mater. Interfaces* **2013**, *5*, 3867−3874.
(52) Hu, X.; Zhou, Q. Health and Ecosystem Risks of Graphene. *Chem. Rev.* **2013**, *113*, 3815−3835.
(53) Ding, X.; Zhao, K.; Zhang, L. Enhanced Photocatalytic Removal of Sodium Pentachlorophenate with Self-Doped Bi_2WO_6 under Visible Light by Generating More Superoxide Ions. *Environ. Sci. Technol.* **2014**, *48*, 5823−3581.
(54) Ma, S.; Zhan, S.; Jia, Y.; Zhou, Q. Superior Antibacterial Activity of Fe_3O_4-TiO_2 Nanosheets under Solar Light. *ACS Appl. Mater. Interfaces* **2015**, *7*, 21875−21883.
(55) Li, H.; Liu, Y.; Cui, Y.; Zhang, W.; Fu, C.; Wang, X. Facile Synthesis and Enhanced Visible-Light Photoactivity of $DyVO_4$/g-C_3N_4I Composite Semiconductors. *Appl. Catal., B* **2016**, *183*, 426−432.

DOI: 10.1021/acssuschemeng.7b01431
ACS Sustainable Chem. Eng. XXXX, XXX, XXX−XXX